The Cap1–claudin-4 regulatory pathway is important for renal chloride reabsorption and blood pressure regulation

Yongfeng Gong[a,b,c], Miao Yu[d], Jing Yang[a,b], Ernie Gonzales[e], Ronaldo Perez[e], Mingli Hou[f], Piyush Tripathi[a], Kathleen S. Hering-Smith[d], L. Lee Hamm[d,1], and Jianghui Hou[a,b,1]

[a]Department of Internal Medicine–Renal Division, [b]Center for Investigation of Membrane Excitability Diseases, and [e]Department of Neurology, Washington University Medical School, St Louis, MO 63110; [c]Department of Physiology, Binzhou Medical College, Yantai 264003, China; [d]Department of Medicine, Tulane University Health Science Center, New Orleans, LA 70112; and [f]Department of Neurobiology, Harvard Medical School, Boston, MA 02115

Edited by David W. Russell, University of Texas Southwestern Medical Center, Dallas, TX, and approved August 8, 2014 (received for review April 14, 2014)

The paracellular pathway through the tight junction provides an important route for transepithelial chloride reabsorption in the kidney, which regulates extracellular salt content and blood pressure. Defects in paracellular chloride reabsorption may in theory cause deregulation of blood pressure. However, there is no evidence to prove this theory or to demonstrate the in vivo role of the paracellular pathway in renal chloride handling. Here, using a tissue-specific KO approach, we have revealed a chloride transport pathway in the kidney that requires the tight junction molecule claudin-4. The collecting duct-specific claudin-4 KO animals developed hypotension, hypochloremia, and metabolic alkalosis due to profound renal wasting of chloride. The claudin-4–mediated chloride conductance can be regulated endogenously by a protease—channel-activating protease 1 (cap1). Mechanistically, cap1 regulates claudin-4 intercellular interaction and membrane stability. A putative cap1 cleavage site has been identified in the second extracellular loop of claudin-4, mutation of which abolished its regulation by cap1. The cap1 effects on paracellular chloride permeation can be extended to other proteases such as trypsin, suggesting a general mechanism may also exist for proteases to regulate the tight junction permeabilities. Together, we have discovered a theory that paracellular chloride permeability is physiologically regulated and essential to renal salt homeostasis and blood pressure control.

chloride channel | epithelium | hypertension

Chloride is the most abundant extracellular anion and thereby determines extracellular fluid volume (ECFV) and blood pressure (BP) (1, 2). The kidney plays a vital role in ECFV and BP control through complex regulatory mechanisms acting upon ion channels and transporters located in the aldosterone-sensitive distal nephron (ASDN) (3, 4). The ASDN comprises the distal convoluted tubule (DCT), the connecting tubule (CNT), and the collecting duct (CD). The primary chloride transport mechanism in the DCT is through the thiazide-sensitive Na^+/Cl^- cotransporter (NCC) to reabsorb Cl^- coupled with equal moles of Na^+ (5). The chloride transport mechanism in the CNT and CD, on the other hand, has been under debate for many years. Recent advances have identified an electroneutral transport pathway for chloride using the Cl^-/bicarbonate exchanger (Slc26a4; pendrin) (6) and the Na^+-driven Cl^-/bicarbonate exchanger (Slc4a8; NDCBE) (7) in the β-intercalated cells (ICs) of CNT and CD. However, such an electroneutral pathway is not able to couple Cl^- reabsorption with epithelial sodium channel (ENaC)-based Na^+ reabsorption that takes place in the principal cells (PCs) of CNT and CD (8), despite many efforts to connect ENaC and pendrin gene expression through endocrine or paracrine mechanisms (9, 10). We and others have previously demonstrated the presence of a paracellular Cl^- pathway or "chloride shunt" in vitro in the CNT and CD cells (11, 12). The paracellular Cl^- channel is made of a key claudin molecule, claudin-4, within the tight junction (TJ) (11). Here, using a tissue-specific KO approach, we have provided conclusive evidence that claudin-4 is required for renal reabsorption of Cl^-; loss of claudin-4 in a transgenic mouse model claudin-$4^{flox/flox}$/$Aqp2^{Cre}$ caused significant renal wasting of chloride, sodium, and volume.

The claudins are a 28-member family of tetraspan proteins that range in molecular mass from 20 to 28 kDa and form a class of ion channels oriented perpendicular to the membrane plane and connecting two extracellular compartments, known as the paracellular channel (13). Claudins associate by *cis* interactions within the plasma membrane of the same cell followed by *trans* interactions between neighboring cells to assemble them in the TJ. Previously, we have observed the *cis* interaction between claudin-4 and claudin-8 and demonstrated that their interaction was required for TJ assembly (11). How claudins *trans* interact, on the other hand, is poorly understood. Here, using several biochemical and imaging criteria, we have found a protease, channel-activating protease 1 (cap1), that transiently disrupted the claudin-4 interaction. Loss of claudin-4 interaction reduced its plasma membrane stability and abundance. Cap1 was the first of several membrane-tethered serine proteases found to activate the amiloride-sensitive ENaC in the ASDN (14, 15). In aldosterone-infused animals, the renal expression levels of cap1 were profoundly elevated, accompanied by increases in the CD Na^+ uptake (16). Despite considerable evidence regarding cap1 regulation of the Na^+ transport in ASDN, it is not known what role cap1 may play in the Cl^- handling. Here, using molecular and electrophysiological approaches, we have revealed how cap1 regulates claudin-4–dependent paracellular Cl^- permeation in the CD.

Significance

How the kidney handles chloride reabsorption has long been a mystery. Here, we have discovered a pathway in the kidney that utilizes channel-activating protease 1 and claudin-4 to physiologically regulate tight junction permeability to chloride. Such a pathway not only is important in renal regulation of chloride but also may play key roles in chloride transport across many other epithelia such as the lung, the salivary gland, and the skin. This discovery also attests to a concept of "druggable" tight junction. Proteases or protease-dependent mechanisms may be developed as pharmacological tools to transiently regulate tight junction permeability in the kidney, the intestine, and the blood–brain barrier.

Author contributions: L.L.H. and J.H. designed research; Y.G., M.Y., J.Y., E.G., R.P., M.H., P.T., and J.H. performed research; Y.G., M.Y., K.S.H.-S., L.L.H., and J.H. analyzed data; and Y.G. and J.H. wrote the paper.

The authors declare no conflict of interest.

This article is a PNAS Direct Submission.

[1]To whom correspondence may be addressed. Email: jhou@wustl.edu or lhamm@tulane.edu.

This article contains supporting information online at www.pnas.org/lookup/suppl/doi:10.1073/pnas.1406741111/-/DCSupplemental.

Results

Generation of CD-Specific KO Animals of Claudin-4. To definitively demonstrate the presence of a chloride shunt in the ASDN and its role in extracellular Cl^- homeostasis in vivo, we have generated the claudin-4 KO animals using homologous recombination. Because claudin-4 is expressed in many epithelia in addition to the ASDN throughout the body, including the skin (17), the intestine (18), the lung (19), the urinary tract (20), and so forth, and constitutive KO of claudin-4 resulted in lethal hydronephrosis due to urothelial hyperplasia (20), we reckon delineation of the claudin-4's role in ASDN will require the Cre-loxP recombination strategy to generate renal tubule-specific deletion. *SI Appendix*, Fig. S1*A* shows the wild-type claudin-4 locus, the targeting construct, and the targeted locus. The exon 1 (only coding exon) of claudin-4 is flanked by two loxP sites. The phosphoglycerate kinase (PGK)-neo expression cassette is flanked by two flippase (flp) recognition target sites. The correctly targeted ES cell clones (*SI Appendix*, Fig. S1 *B–D*) all showed normal karyotypes and were injected into the C57BL/6 blastocysts to generate chimera founders. The targeted allele was captured in the F1 generation derived from all chimera founders (*SI Appendix*, Fig. S1*E*), indicating successful germ-line transmission. Cleavage of PGK-neo was carried out by crossing F1 with a transgenic mouse line (129S4/SvJaeSor-Gt[reverse orientation splice acceptor (ROSA)]26Sor; the Jackson Lab) that expresses the flp recombinase in the ROSA locus (*SI Appendix*, Fig. S1*E*). Capture of both floxed alleles was achieved by the intercross of claudin-$4^{flox/+}$ heterozygous animals that had been backcrossed to the C57BL/6 background for five generations (*SI Appendix*, Fig. S1*E*). The claudin-$4^{flox/flox}$ animals were then crossed to the $Aqp2^{Cre}$ hemizygous transgenic mice [established on a C57BL/6 background; B6.Cg-Tg(Aqp2-cre)1Dek/J; the Jackson Lab] that expressed the Cre recombinase under the Aquaporin-2 (Aqp2) promoter in the PCs of the CNT and CD.

Because the nephron is an axial segmental system made of heterogeneous epithelia—the proximal tubule (PT), the thin limb (TL), thick ascending limb (TAL) of the Henle's loop, the DCT, the CNT, and the CD (*SI Appendix*, Fig. S2*A*)—a definitive determination of claudin-4 cellular localization is essential to its functional study (Fig. 1 and *SI Appendix*, Figs. S2 and S3). Through rigorous colocalization analyses, we found that in claudin-$4^{flox/flox}$ (control) mouse kidneys, claudin-4 proteins were detected in tubules absent of the *Lotus tetragonolobus* lectin (a proximal convoluted/straight tubule marker) (*SI Appendix*, Fig. S2*B*) but coexpressing Aqp1 (a TL marker) in the medulla (*SI Appendix*, Fig. S2*C*). The TAL and the early portion of DCT (DCT1) were without claudin-4, revealed by the lack of colocalization between claudin-4 and $Na^+/K^+/Cl^-$-cotransporter 2 (NKCC2; a TAL marker) (*SI Appendix*, Fig. S2*D*) or NCC (a DCT marker) (*SI Appendix*, Fig. S2*E*). Claudin-4 expression was turned on from the late portion of DCT (DCT2) (*SI Appendix*, Fig. S2*E*) and extended to the CNT and CD that were counterstained with Aqp2 (a CNT/CD marker) (Fig. 1*A*). The CNT/CD itself is a heterogeneous epithelium, made of the PC and the IC. With markers unique to each cell type, we found that (*i*) the majority of cell–cell junctions made of claudin-4 were between the PCs (counterstained with Aqp2, a PC marker) (Fig. 1*B*)—the homotypic junction; (*ii*) claudin-4 can be found in cell junctions between the ICs (counterstained with pendrin, an IC cell) (Fig. 1*C*); and (*iii*) claudin-4 can also be found in cell junctions between PC and IC cells (Fig. 1 *B* and *C*)—the heterotypic junction. Aqp2 is expressed along the CNT and CD (*SI Appendix*, Fig. S3*A*) (21); the $Aqp2^{Cre}$ transgenic mice have been successfully used to generate the CNT/CD-specific KO of ENaC (22) and mineralocorticoid receptor (23). In claudin-$4^{flox/flox}$/$Aqp2^{Cre}$ mice, the claudin-4 expression in TL and DCT2 was not affected, revealed by clear colocalization with Aqp1 (*SI Appendix*, Fig. S3*B*) and NCC (*SI Appendix*, Fig. S3*C*), respectively. The Aqp2-positive tubules were, however, depleted with claudin-4 proteins (Fig. 1*D*). Because Aqp2 is only expressed by the PC cell (21), the Aqp2-negative IC cells retained claudin-4 expression (Fig. 1 *E* and *F*). The cell junctions made between IC cells (Fig. 1*E*), IC–PC cells (Fig. 1*F*), but not PC–PC cells (Fig. 1 *E* and *F*) were stained with claudin-4, indicating an IC origin of claudin-4 expression. Histological analyses revealed no morphological abnormality in the CNT/CD. Together, these results have demonstrated successful deletion of the claudin-4 gene in a renal tubule-specific manner.

Claudin-4 KO Animals Developed Renal Loss of Cl^- and Low BP. The age-matched (10–12-wk-old) CNT/CD-specific KO of claudin-4 (claudin-$4^{flox/flox}$/$Aqp2^{Cre}$) and its control mice (claudin-$4^{flox/flox}$) were maintained on a regular salt diet (0.24% Na^+, 0.30% Cl^-;

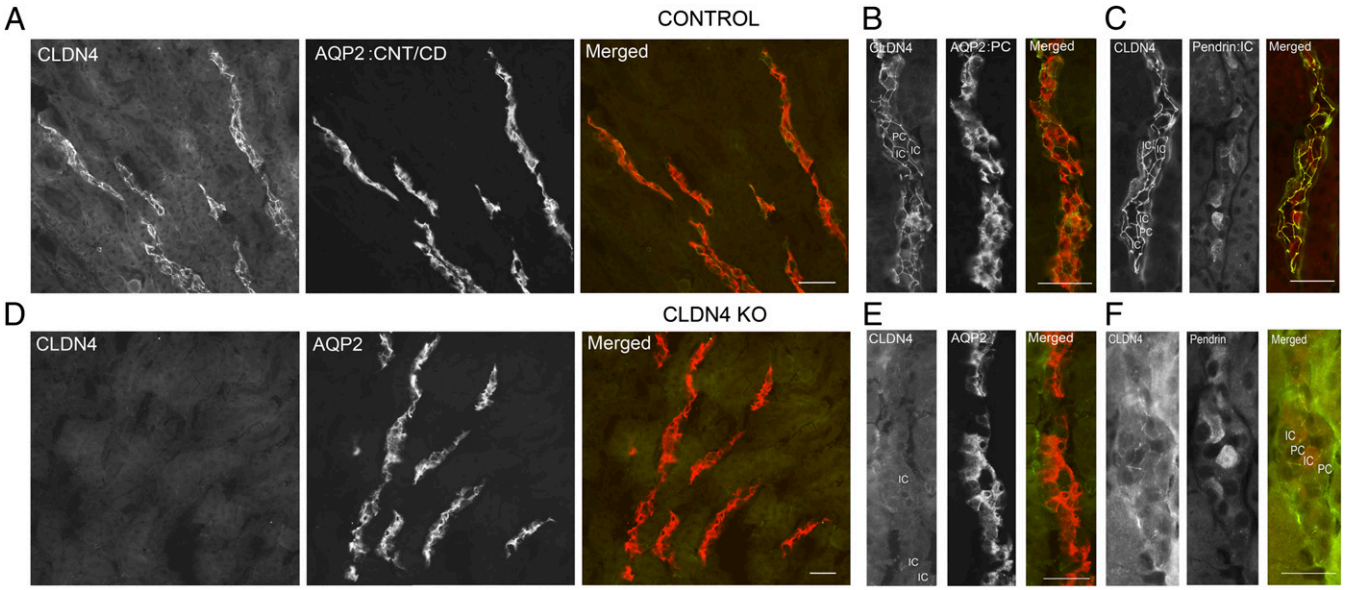

Fig. 1. CLDN4 cellular localization pattern in control (*A–C*) and Aqp2-Cre–driven KO (*D–F*) mouse kidneys. (*A* and *D*) Double staining of CLDN4 with a CNT/CD marker, Aqp2, in the cortical medullar ray from the OSOM to cortex. (*B* and *E*) Double staining of CLDN4 with a PC marker, Aqp2, in the CNT/CD of the cortex. IC, intercalated cell; PC, principal cell. (*C* and *F*) Double staining of CLDN4 with an IC marker, pendrin, in the CNT/CD of the cortex. CD, collecting duct; CNT, connecting tubule; OSOM, outer stripe of outer medulla. (Scale bar in all images, 20 μm.).

SI Appendix, SI Materials and Methods) and subjected to 24-h metabolic cage analyses. No difference was observed in body weight between KO and control animals (Table 1). The plasma Cl^- level in KO was significantly lower than in control animals (Table 1). This was caused by profound renal loss of Cl^- in KO animals: fractional excretion of Cl^- (FE_{Cl}) increased by 1.79-fold, and absolute excretion of Cl^- (E_{Cl}) increased by 1.96-fold, compared with controls (Table 1). The circulating Na^+ (P_{Na}) level was well defended by the KO animals, despite their significant renal loss of Na^+: FE_{Na} and E_{Na} were 1.52-fold and 1.66-fold higher than control (Table 1). The plasma K^+ level (P_K) in KO animals showed a clear trend toward hyperkalemia; the renal handling of K^+ (FE_K and E_K) was not significantly different between KO and control animals (Table 1). The urinary volume (UV) in KO was significantly higher than in control mice, despite similar glomerular filtration rates (GFRs) between the two genotypes (Table 1), suggesting a volume loss through the distal nephron origin. The volume loss was secondary to the salt loss because the urinary osmotic pressure was not changed in KO animals (Table 1). To record BP in anesthetized animals, we catheterized the carotid artery and performed intra-arterial measurements. The mean BP in KO was significantly lower than in control mice (Table 1), compatible with the renal loss of volume. To record BP in unanesthetized and unrestrained animals, sex- (male) and age- (12-wk-old) matched KO and littermate control mice were implanted with radiotelemetric transducers in the carotid artery (*SI Appendix, Materials and Methods*). Telemetric traces of their mean BP levels over a 24-h period were shown in Fig. 2. The mean BP in KO was consistently lower than in control animals throughout the 24-h period; the difference was significant during the dark cycle. The arterial pH in KO animals was maintained at a similar level to control, even though their arterial HCO_3^- levels (P_{HCO3}) were significantly higher than control (Table 1), indicating compensated metabolic alkalosis. The urine pH levels were similar between control and KO animals (Table 1). The renin–angiotensin–aldosterone (RAA) axis was carefully monitored for both genotypes. The KO and control animals were homozygous for a single renin allele (*Ren1*^{c}; C57BL/6 background) (24); primers against the *Ren1*^{c} gene allowed quantitative RT-PCR analyses of renin gene expression in the kidney. The renal renin expression levels were unchanged between KO and control animals (*SI Appendix*, Fig. S4*A*), nor was there any change in the plasma angiotensin-II (*SI Appendix*, Fig. S4*B*) or aldosterone levels (*SI Appendix*, Fig. S5).

The lack of RAA response in claudin-4 KO animals under regular diet prompted us to ask whether dietary salt restriction might unmask the KO effects on ECFV and BP deregulation. Age-matched (10–12-wk-old) KO and control animals were maintained on a low-salt diet (0.03% Na^+, 0.05% Cl^-; *SI Appendix, Materials and Methods*) for 5 consecutive days and subjected to 24-h metabolic cage analyses on the sixth day. A significant decrease was found in body weight of KO compared with control mice (Table 1). The UV loss in KO was more severe under a low-salt diet (by 53%) than under a regular diet (by 31%) (Table 1). The hypotension in KO was also exacerbated by low-salt treatment, with mean BP difference reaching 13.8 mmHg in anesthetized animals (Table 1), whereas a regular diet only induced a 6.5 mmHg difference. The hematocrit level was significantly higher in KO animals fed with a low-salt diet but not with a regular diet (Table 1). The hypochloremia (P_{Cl}), chloriuresis (FE_{Cl} and E_{Cl}), and natriuresis (FE_{Na} and E_{Na}) of KO mice were retained under a low-salt diet (Table 1); notably, the reduction of urinary salt excretion (FE_{Cl} and FE_{Na}) was slower in KO from regular to low-salt dietary treatments (Table 1), indicating defects in low-salt–induced renal reabsorption. Consistent with this finding, the plasma aldosterone levels now became markedly higher in KO animals (*SI Appendix*, Fig. S5), suggesting that the blunted salt reabsorption in the ASDN must be compensated with increased aldosterone production. Similar to a regular dietary condition, there was no difference in GFR, urinary osmotic pressure, or renal handling of K^+ between the two genotypes under a low-salt treatment (Table 1). Together, these results have revealed a key role of the paracellular pathway in renal salt reabsorption and BP regulation.

Trypsin Decreases Paracellular Cl^- Conductance in the CD. Liu et al. first noticed that aprotinin, a peptide inhibitor for trypsin, when added to the apical side of the mouse CD M-1 cells, reduced not only the amiloride-sensitive Na^+ current (I_{eq}) but also the transepithelial resistance (TER), an inverse indicator for paracellular conductance (25). The serine protease trypsin reversed the aprotinin effects on I_{eq} and TER. These earlier efforts raised

Table 1. Plasma and urine electrolyte levels in claudin-4 KO and its control animals under a regular or low-salt diet

	Regular diet			Low-salt diet		
Measure	CLDN4$^{flox/flox}$	CLDN4$^{flox/flox}$/Aqp2^{Cre}	Significance, $n = 15$	CLDN4$^{flox/flox}$	CLDN4$^{flox/flox}$/Aqp2^{Cre}	Significance, $n = 8$
Weight, g	20.94 ± 0.64	20.08 ± 0.40	n.s.	21.35 ± 0.86	18.89 ± 0.29	$P = 0.044$
UV, µL/24 h g	46.01 ± 3.21	60.32 ± 4.21	$P = 0.012$	27.06 ± 4.03	41.27 ± 3.79	$P = 0.022$
Osm, Osm/kg H_2O	1.653 ± 0.066	1.815 ± 0.101	n.s.	1.42 ± 0.08	1.25 ± 0.08	n.s.
Urine pH*	6.06 ± 0.10	6.13 ± 0.24	n.s.	–	–	–
GFR, ml/24 h g	3.07 ± 0.35	3.29 ± 0.30	n.s.	2.59 ± 0.36	2.41 ± 0.23	n.s.
Hematocrit, %†	47.3 ± 0.8	48.9 ± 1.0	n.s.	48.6 ± 0.4	50.4 ± 0.4	$P = 0.007$
Mean BP, mmHg	95.2 ± 2.5	88.7 ± 1.4	$P = 0.036$	95.6 ± 2.4	81.8 ± 2.3	$P = 0.003$
Serum pH	7.43 ± 0.01	7.44 ± 0.01	n.s.	–	–	–
$pHCO_3$, mmol/L	22.5 ± 0.8	25.0 ± 0.9	$P = 0.045$	–	–	–
P_{Cl}, mmol/L	105.0 ± 0.9	101.1 ± 1.4	$P = 0.022$	108.9 ± 0.6	106.4 ± 0.7	$P = 0.020$
P_{Na}, mmol/L	142.3 ± 0.9	145.8 ± 2.2	n.s.	142.2 ± 2.1	143.4 ± 1.4	n.s.
P_K, mmol/L	3.85 ± 0.16	4.28 ± 0.14	$P = 0.060$	3.96 ± 0.16	3.81 ± 0.11	n.s.
FE_{Cl}, %	1.30 ± 0.18	2.33 ± 0.26	$P = 0.003$	0.57 ± 0.03	1.36 ± 0.15	$P = 0.0001$
E_{Cl}, µmol/24 h g	3.71 ± 0.42	7.27 ± 0.84	$P = 0.0007$	1.57 ± 0.20	3.32 ± 0.28	$P = 0.0002$
FE_{Na}, %	0.81 ± 0.11	1.23 ± 0.13	$P = 0.022$	0.27 ± 0.05	0.67 ± 0.07	$P = 0.0003$
E_{Na}, µmol/24 h g	3.10 ± 0.33	5.15 ± 0.55	$P = 0.004$	0.97 ± 0.21	2.22 ± 0.19	$P = 0.0008$
FE_K, %	18.74 ± 1.74	19.60 ± 3.09	n.s.	17.42 ± 1.60	23.92 ± 3.69	n.s.
E_K, µmol/24 h g	1.93 ± 0.15	2.39 ± 0.23	n.s.	1.60 ± 0.22	1.96 ± 0.26	n.s.

*Spot urine collection ($n = 8$).

†In sex-matched (male) animals, $n = 7$. BP, blood pressure; E_{Cl}, absolute excretion level of Cl^-; E_K, absolute excretion level of K^+; E_{Na}, absolute excretion level of Na^+; FE_{Cl}, fractional excretion level of Cl^-; FE_K, fractional excretion level of K^+; FE_{Na}, fractional excretion level of Na^+; GFR, glomerular filtration rate; Osm, osmotic pressure; P_{Cl}, plasma Cl^- level; P_{HCO3}, plasma HCO_3^- level; P_K, plasma K^+ level; P_{Na}, plasma Na^+ level; UV, urinary volume.

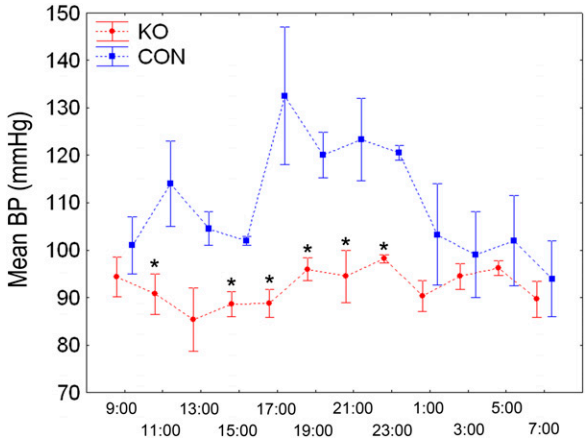

Fig. 2. In vivo telemetric BP recording comparing KO and littermate control animals over a 24-h period. Data are presented as the mean arterial pressure ± SEM over time at 2-h intervals. *$P < 0.05$, $n = 3$.

a tantalizing possibility that the paracellular transport, presumably Cl^-, could also be regulated by proteases such as trypsin. In continuity with these previous studies, we used the native mouse CD cells as the research model (e.g., the cortical CD cell M-1 and the inner medullar CD cell mIMCD3) that retained most of the in vivo physiological features of the CD, such as the amiloride-sensitive Na^+ current and the paracellular Cl^- conductance. To record precise paracellular permeabilities, we used a mixture of transcellular ion channel inhibitors to block transcellular conductance (*SI Appendix, Materials and Methods*; amiloride for ENaC, bumetanide for NKCC1, DIDS for anion channels, and niflumic acid for pendrin). Because the CD cell possessed endogenous protease activity (16), we pretreated the M-1 and mIMCD3 cell monolayers with the protease inhibitor aprotinin at 20 μg/mL to the apical side for 2 h as described by Liu et al. (25). The trypsin effects were fast; TER was already significantly increased 1.70-fold and 1.97-fold in M-1 and mIMCD3 cells, respectively, by 20 μg/mL trypsin when added to the apical side for 20 min (Fig. 3*A*). The voltage-current curve was linear in the presence and absence of trypsin, suggesting a paracellular effect. To reveal the changes in paracellular ion selectivity, we performed dilution potential (DP) measurements as described by Hou et al. (11) (with the apical side as zero reference; *SI Appendix, Materials and Methods*). The DP induced by the transepithelial NaCl gradient allowed the calculation of anion selectivity (P_{Cl}/P_{Na}) according to the Goldman–Hodgkin–Katz equation. In aprotinin-pretreated M-1 cells, trypsin significantly increased DP at 20 min (Fig. 3*B* and *SI Appendix*, Table S1), which reflected a pronounced reduction in anion selectivity (Fig. 3*C* and *SI Appendix*, Table S1). The decrease in anion selectivity was primarily due to inhibition of paracellular Cl^- permeation (Fig. 3*D* and *SI Appendix*, Table S1), although P_{Na} was also significantly reduced (*SI Appendix*, Table S1). The trypsin effects were reproducible in another CD cell culture—mIMCD3. Trypsin, at the same dose and time point, significantly increased DP (Fig. 3*B* and *SI Appendix*, Table S1), which derived from decreases in anion selectivity (Fig. 3*C* and *SI Appendix*, Table S1) and P_{Cl} (Fig. 3*D* and *SI Appendix*, Table S1). Together, these results have revealed a previously unknown aspect of trypsin's role in CD epithelia—modulation of paracellular Cl^- transport.

RNA Interference Reveals an Endogenous Regulator of Paracellular Cl^- Conductance in the CD—cap1. The renal expression profile of cap1—a trypsin-like protease—had been determined by Vuagniaux et al. using microdissected tubules: the PT showed the most predominant expression, followed by substantial expression in the TAL of Henle's loop and the CD (26). Because cap1 was secreted into the tubular lumen (16), its expression in renal tubules proximal to the CD would suggest a paracrine role, whereas its expression in the CD per se would suggest an autocrine role. To reveal the autocrine function of cap1 in the CD, we generated transgenic M-1 and mIMCD3 cells expressing small interference RNA (siRNA) molecules against cap1 mRNA, as described by Hou et al. (11). The siRNA molecules were designed by the siDESIGN center at Thermo Scientific, and each contained a unique complementary 19-nucleotide sequence within the coding region of the mouse cap1 gene. Three independent siRNA sequences (561, 829, and 849; *SI Appendix*, Table S4) were tested in M-1 and mIMCD3 cells. As we aimed to have cap1 expression suppressed by siRNAs during a prolonged period in polarized CD cells, we used a previously described retroviral siRNA expression system (pSIREN; *SI Appendix, Materials and Methods*) capable of infecting a wide range of host cells and integrating into their genomes (27). Because cap1 was secreted protein not found in the cell lysate (16) (*vide infra*), we reckoned that measurements on the mRNA level would provide a more faithful determination of the siRNA knockdown (KD) efficacy. All three siRNAs reduced cap1 mRNA levels significantly by 44% for 561, 50% for 829, and 84% for 849 compared with scrambled siRNA in M-1 cells (normalized to β-actin mRNA; *SI Appendix*, Fig. S6). Because 849 demonstrated the most effective KD, we recorded TER, DP, P_{Cl}/P_{Na}, and P_{Cl} in 849-infected M-1 and mIMCD3 cells. Transcellular ion channel inhibitors were included during recording as described elsewhere in this study. In both M-1 and mIMCD3 cells, the KD of cap1 significantly reduced the TER (Fig. 4*A* and *SI Appendix*, Table S2). The most telling finding was the change in junctional DP (Fig. 4*B* and *SI Appendix*, Table S2) and ion selectivity (Fig. 4*C* and *SI Appendix*, Table S2). The baseline level of slightly cation-selective TJ in M-1 and mIMCD3 cells became highly anion selective, reflected by the reversal of junctional DPs. The changes in ion selectivity were due to significant increases in P_{Cl} (by 2.03-fold in the M-1 cell and 1.89-fold in the mIMCD3 cell; Fig. 4*D* and *SI Appendix*, Table S2), whereas P_{Na} was not significantly affected. Together, these results have pointed to an endogenous proteolytic pathway in the CD that acts to regulate paracellular Cl^- conductance.

Claudin-4 Is Required for cap1-Dependent Regulation of Paracellular Cl^- Transport. Because cap1 is predominantly expressed in the PT (26), it could play a paracrine role in the CD through constant secretion into the preurine as a carrier. The most straightforward approach to this hypothesis is by using recombinant cap1 proteins in the apical solution of CD cells during recording. Knowing that the cap1 zymogen requires activation by cleavage at Arg44–Ile45 (28), generating a disulfide-linked active form that is further cleaved at the glycosylphosphatidylinositol anchor site (29), we used the HEK293 cells instead of *Escherichia coli* to produce active recombinant cap1 proteins (*SI Appendix, Materials and Methods*). To maintain a constant dosage of cap1 throughout multiple recordings, the recombinant cap1 protein levels from HEK293 cell-producing medium were quantified with Western blot against a cap1 protein standard (*SI Appendix*, Fig. S7) and adjusted to 100 nM in the apical solutions of the recorded cells. The control cells received HEK293 cell medium transfected with an empty vector. To remove endogenous cap1 activity, the M-1 and mIMCD3 cell monolayers were pretreated with aprotinin as described elsewhere in this study. The inhibitor mixture for transcellular ion channels was used, as described for previous recordings. In many ways similar to trypsin, cap1 significantly increased the TER by 1.43-fold and 1.36-fold in M-1 and mIMCD3 cells, respectively, after 20 min of treatment (Fig. 5*A* and *SI Appendix*, Table S3), even though the fold of increase was not as high as with trypsin (Fig. 3*A*). The DPs in both M-1 and mIMCD3 cells were significantly increased by cap1 (Fig. 5*B* and *SI Appendix*, Table S3), resulting in a significant drop in anion selectivity (Fig. 5*C* and *SI Appendix*, Table S3) and P_{Cl} (Fig. 5*D* and *SI Appendix*, Table S3). The P_{Cl} in cap1-treated M-1 cells was similar to that in trypsin-treated cells, but cap1 was less potent than trypsin to repress P_{Cl} in mIMCD3 cells (Fig. 3*D*). Notably, in contrast to trypsin, cap1 had

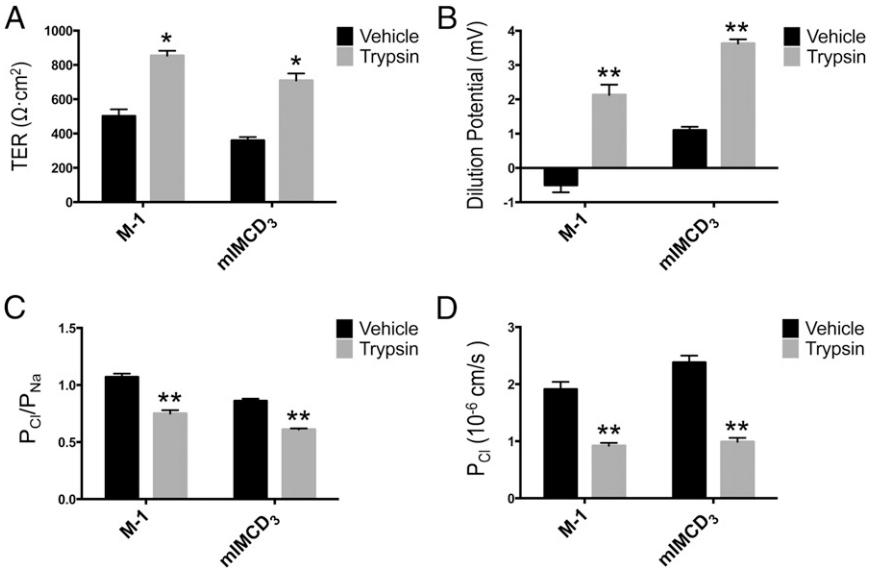

Fig. 3. Effects of trypsin on paracellular ion permeation. Transient ectopic trypsin treatments in the apical membrane altered TER (*A*), DP (*B*), anion selectivity (P_{Cl}/P_{Na}) (*C*), and Cl^- permeability (P_{Cl}) (*D*) across the M-1 and mIMCD3 cell monolayers. $*P < 0.05$; $**P < 0.01$ relative to vehicle treatment, $n = 3$.

no effect on P_{Na} (*SI Appendix*, Table S3), suggesting cap1 was a more specific modulator of TJ. We have previously identified the molecular component underlying paracellular Cl^- permeation, claudin-4, from the CD cells using RNA interference (11). Next, we asked whether cap1 acted through claudin-4. The claudin-4 KD cells were generated as described before (11). Consistent with previous recordings, the claudin-4 KD cells reduced P_{Cl} in both M-1 and mIMCD3 cells (*SI Appendix*, Table S3). In M-1::claudin-4 KD cells, cap1 failed to alter TER (Fig. 5*A*), DP (Fig. 5*B*), ion selectivity (Fig. 5*C*), and P_{Cl} (Fig. 5*D*). The baseline P_{Cl} level in KD cells was similar to that in WT cells with cap1 treatment (Fig. 5*D*), suggesting the cap1 pathway was very effective in shutting down the chloride shunt in the cortical CD cells. The cap1 effects on TER (Fig. 5*A*), DP (Fig. 5*B*), ion selectivity (Fig. 5*C*), and P_{Cl} (Fig. 5*D*) were also abolished in mIMCD3::claudin-4 KD cells. The baseline level of P_{Cl} in KD cells was far lower than that of cap1-treated WT cells (Fig. 5*D*), suggesting incomplete shutdown of chloride shunt by cap1 in the inner medullar CD cells. Together, these results have revealed an important molecular axis, cap1–claudin-4, in the CD underpinning the physiological regulation of chloride shunt.

Cap1 Regulates claudin-4 *trans* Interaction and Cell Surface Stability. Knowing that cap1 regulated claudin-4–dependent paracellular Cl^- permeation, we asked what mechanism cap1 may use to control claudin-4. Because the cap1 effect was fast—within 20 min—it would be less likely caused by changes in claudin-4 gene expression levels or through complex signaling cascades such as the protease-activated receptor (PAR) signaling (30). Instead, claudin interactions, which had been shown to play a crucial role in claudin-16 and -19 permeability (31, 32), became the most tangible hypothesis. Claudins interact with one another both intracellularly and intercellularly (33). In the formation of the intercellular junction, claudins *trans* interact between adjacent cells, sealing off the paracellular space. Because cap1 acted upon claudin-4 extracellularly, we began with testing how cap1 affected claudin-4 intercellular interaction. Due to the remarkably complex biochemical structure of TJ, claudin interactions, especially the *trans* interaction in mature epithelial cells such as MDCK or M-1 cells, may be difficult to delineate due to many other protein interactions within the TJ matrix. To study selective claudin interactions, we used the simple cell systems such as the

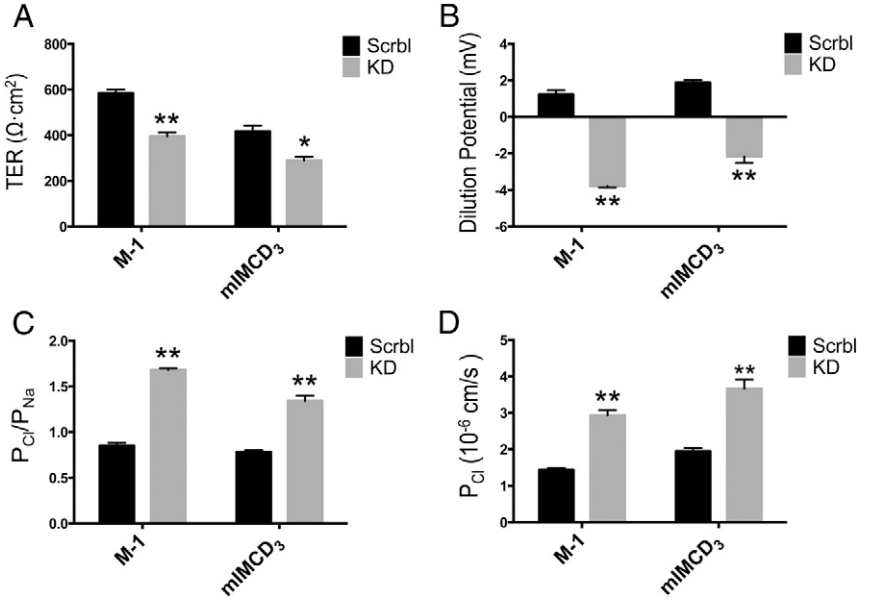

Fig. 4. Effects of cap1 KD on paracellular ion permeation. Chronic cap1 KD mediated by siRNA849 altered TER (*A*), DP (*B*), anion selectivity (P_{Cl}/P_{Na}) (*C*), and Cl^- permeability (P_{Cl}) (*D*) across the M-1 and mIMCD3 cell monolayers. $*P < 0.05$; $**P < 0.01$ relative to scrambled siRNA, $n = 3$.

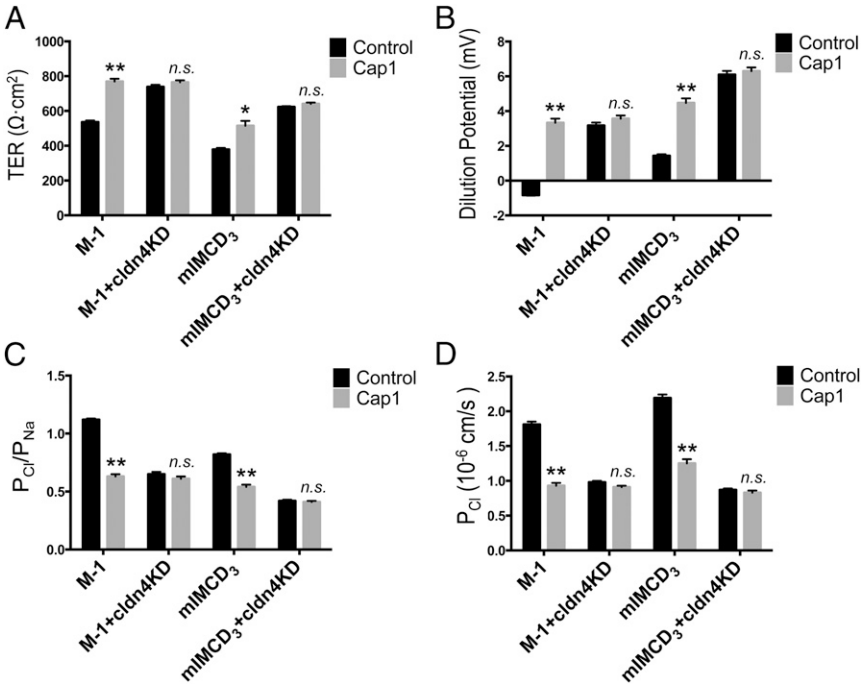

Fig. 5. Effects of recombinant cap1 on paracellular ion permeation and the claudin-4 dependence. Transient recombinant cap1 treatments in the apical membrane altered TER (*A*), DP (*B*), anion selectivity (P_{Cl}/P_{Na}) (*C*), and Cl^- permeability (P_{Cl}) (*D*) across the M-1 and mIMCD3 cell monolayers. These effects were abolished in claudin-4 KD cells receiving the same cap1 treatment. $*P < 0.05$; $**P < 0.01$ relative to control treatment (HEK293 cell medium receiving empty vector transfection), $n = 3$.

fibroblasts (mouse L cells) and the premature epithelial cells (HEK293 cells) that formed no TJ and expressed no endogenous claudin. We applied two criteria—coimmunoprecipitation (CoIP) and colocalization—to quantitatively reveal claudin interaction. The CoIP approach was first used by Daugherty et al. (34) to probe the claudin-3 and -5 *trans* interaction. To differentiate the claudin-4 molecules on two adjacent cells, we made two expression constructs in which a His epitope tag or a GFP protein tag was appended to the N terminus of the claudin-4 molecule, knowing that tagging at the N terminus of claudin would not affect its trafficking or function (27). The His–claudin-4 or GFP–claudin-4 was transfected into mouse L cells independently, and the transfected cells were then cocultured to form cell–cell contacts. The plasma membrane proteins were extracted using a centrifugal approach as described before (*SI Appendix*, *Materials and Methods*) (31). Immunoblots showed that anti-His antibody, but not anti–claudin-1 (as the nonspecific binding control), was able to precipitate GFP–claudin-4 in the absence of cap1 (*SI Appendix*, Fig. S8). The precipitated claudin-4 levels were normalized to its surface membrane abundance level, mindful that the membrane abundance itself could be variable due to cap1 regulation (*vide infra*). Addition of recombinant cap1 to the medium for 1 h (purified from HEK293 cells and equivalent to the 100 nM standard described elsewhere in this study) clearly diminished the precipitated claudin-4 levels in three independent experiments (*SI Appendix*, Fig. S8). Quantitative densitometric analysis revealed significant reduction of the IP/membrane claudin-4 abundance ratio (Fig. 6*A*), indicating decreases in the claudin-4 *trans* interaction. The cap1 effect on the claudin-4 interaction was further confirmed by an imaging approach independently developed by Piontek et al. in the study of claudin-5 interactions (35) and by us in the study of claudin-16 and -19 interactions (31). According to Piontek et al. (35), normal *trans* interactions (or TJ) can be seen as predominant enrichment at HEK293 cell–cell contact transfected with claudin-4 molecules; quantitatively, the signal intensity of claudin-4 immunostaining at cell–cell contacts (Fig. 6 *B*, *i*, arrow) was twofold higher than its plasma membrane levels (Fig. 6 *B*, *i*, arrowhead and *SI Appendix*, Fig. S9*A*). This was clearly not the case when cap1 was present at 100 nM for 1 h. Cap1 rendered claudin-4 distribution homogenous throughout the plasma membrane (Fig. 6 *B*, *ii*), suggesting a loss of *trans* interaction (or disjunction). In addition, a gap can be seen between two adjacent cell membranes (Fig. 6 *B*, *ii*, rectangle) separated by a ∼1 μm distance (*SI Appendix*, Fig. S9*B*), where no cell contact was made. Two-color imaging further revealed a lack of colocalization of claudin-4 molecules from two adjoining cells (Fig. 6 *B*, *iii*). In mature epithelia such as the M-1 cells, claudin-4 molecules were found exclusively in the TJ (Fig. 6*C*). Cap1 treatment, when carried out to the apical surface of M-1 cells at 100 nM for 1 h, dramatically reduced the TJ abundance of claudin-4 proteins (Fig. 6*C*). Intriguingly, the cap1 effect appeared to be exclusive to the bicellular junction, whereas claudin-4 localization in the tricellular junction remained largely intact (Fig. 6*C*, arrow). The gross integrity of TJ was not affected by cap1 in M-1 cells, as shown by intact ZO-1 localization (Fig. 6*C*). Intercellular claudin interactions were known to be important in maintaining its cell surface abundance (35), presumably through clathrin-mediated endocytosis (36). To determine how cap1 affected claudin-4 cell surface abundance, we measured the cell-surface biotinylated claudin-4 levels with membrane-impermeable Sulfo-NHS-SS-biotin labeling (*SI Appendix*, *Materials and Methods*) in three cell models—M-1, mIMCD3, and HEK293. Because M-1 and mIMCD3 cells both expressed the endogenous claudin-4 protein, which integrated into the TJ when grown on Transwell, protein biotinylation was carried out from the apical side. After a pretreatment with the protease inhibitor aprotinin to suppress endogenous cap1 activity, recombinant cap1 at 100 nM and for 1 h markedly reduced the apical surface claudin-4 levels in both M-1 and mIMCD3 cells (Fig. 6*D*). The changes in surface claudin-4 levels were further confirmed in HEK293 cells transfected with exogenous claudin-4 (*SI Appendix*, Fig. S10), suggesting the cap1 effect on claudin-4 membrane stability required no prior TJ formation.

Cap1 may regulate claudin-4 either through direct proteolysis or through proteolysis of its accessory proteins. In general, serine proteases require a basic amino acid—arginine or lysine—at the P1 site on its substrate for cleavage. Positional scanning experiments using combinatorial substrate libraries have revealed the substrate preference for cap1: a tetrabasic site from P4–P1, whereas P1'–P4' showed broad selectivity (37). Because cap1 acts upon claudin-4 from extracellular milieu, its cleavage site must be within the extracellular loops of claudin-4 (ECL1 or ECL2) if claudin-4 is a substrate of cap1. To test this hypothesis, we looked for the basic amino acid sites in claudin-4 ECL1 (R31, K65, and R81; *SI Appendix*, Fig. S10*A*) and ECL2 (K157 and

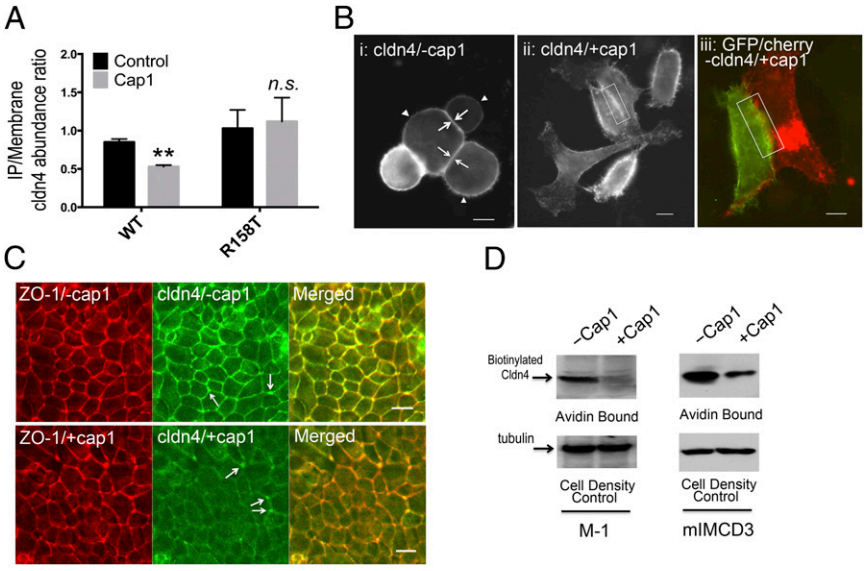

Fig. 6. Effects of recombinant cap1 on claudin-4 interaction and membrane stability. (*A*) Statistic graph showing immunoprecipitated versus membrane claudin-4 protein abundance as measurement of its *trans* interaction strength. $^{**}P < 0.01$, $n = 3$ independent experiments shown in *SI Appendix*, Fig. S8. (*B*) In unpolarized HEK293 cells, claudin-4 protein is predominantly localized at the cell–cell junction (*i*, arrow) and variably at the nonjunctional plasma membrane (*i*, arrowhead). In the presence of cap1, claudin-4 relocated to nonjunctional plasma membrane (rectangle) under single-color (*ii*) and dual-color (*iii*) fluorescence imaging. (Scale bar, 10 μm.) (*C*) In mature M-1 cells, the TJ localization of claudin-4 was dramatically reduced after cap1 treatment. Arrow indicates tricellular junction. (Scale bar, 10 μm.) (*D*) Cell surface membrane biotinylation levels of claudin-4 protein in polarized M-1 and mIMCD3 cells treated with cap1.

R158; *SI Appendix*, Fig. S10*A*), systematically mutated them to threonine (T), and tested the cap1 effect on mutant claudin-4 with the interaction and membrane stability assays developed elsewhere in this study. As the R81T mutation was known to affect claudin-4 protein folding, rendering its mislocalization to the endoplasmic reticulum (11), this site was ruled out initially. Because the R158 site is flanked by a preceding lysine, it represents an ideal cleavage site for cap1, according to Shipway et al. (37). Using the membrane stability assay developed for the HEK293 cell that lacks endogenous claudin-4 and can be transfected with wild-type or mutant claudin-4 for comparison, we have found that mutation at the R158 but not the R31, K65, or K157 site protected claudin-4 from cap1-induced destabilizing on the cell membrane (*SI Appendix*, Fig. S10*B*). Because the K65 site on ECL1 constitutes the paracellular ion-permeating pore (11), it is clear from current data that cap1 does not affect the ion permeation directly; instead it acts through ECL2 and claudin dissociation. Notably, the R158 site is not present in claudin-2, a classic Na^+ channel expressed in the PT, suggesting the specificity of cap1 effects to the distal tubules. To test if the R158 site was involved in cap1-mediated claudin-4 *trans* dissociation, we used the CoIP assay in the mouse L cell described elsewhere in this study. The His–claudin-4–R158T or GFP–claudin-4–R158T was transfected into the L cells separately, followed by coculturing, membrane extraction, and immunoprecipitation. The ability for mutant claudin-4 to form a *trans* interaction was well preserved, as shown by the immunoblot that anti-His but not anti–claudin-1 precipitated GFP–claudin-4–R158T (*SI Appendix*, Fig. S8). In contrast to the wild-type claudin-4, the mutant interaction was not disrupted by cap1 treatment, as revealed by the unchanged IP/membrane ratio (Fig. 6*A*). Immunofluorescence imaging further confirmed this finding that no disjunction was made between mutant claudin-4 in the presence of cap1. Together, these data have revealed a previously unknown mechanism for cap1 to regulate claudin intercellular interaction, membrane stability, and transport function.

Discussion

What is the role of the paracellular Cl^- pathway in renal handling of salt and volume? The primary Na^+ reabsorption pathway in the CNT and CD is via ENaC, which absorbs Na^+ through the luminal membrane of the PC and creates a lumen-negative voltage difference (V_{te}) across the epithelium (*SI Appendix*, Fig. S11). The V_{te} favors Cl^- reabsorption through the TJ; therefore, loss of claudin-4 lowers Cl^- reabsorption, leading to increases in urinary Cl^- excretion and hypochloremia. The chloriuretic phenotype is evident in both the CNT/CD-specific KO mouse described here and the global KO mouse generated by Fujita et al. (20). Accumulation of luminal Cl^- increases the magnitude of V_{te}, depolarizes the apical membrane, and consequently inhibits ENaC (8), causing Na^+-wasting defects similar to the CNT/CD-specific ENaC KO mouse (22). The renal loss of salt and volume is compatible with the hypotensive phenotype of claudin-4 KO. Paradoxically, the RAA system was not significantly activated under basal condition by the loss of claudin-4. There are two explanations: (*i*) The hypotension is very mild, and (*ii*) there is circadian regulation. The telemetry analysis has provided preliminary support to the circadian regulation hypothesis. Notably, several KO models in the WNK1–SPAK/OSR1 pathway have demonstrated similar circadian rhythm-dependent BP phenotypes (38, 39). The circadian clock genes (Cryptochrome-1 and -2) control aldosterone biosynthesis levels that oscillate by about fourfold during the day–night cycle (40). Consistent with this concept, the claudin-4 KO mice showed more severe hypotension when challenged with a low-salt diet. The Cl^- depletion in the extracellular fluid creates anion paucity that is replenished by the intracellular HCO_3^- (41), explaining in part the metabolic alkalosis of claudin-4 KO. No aciduria was found in these animals, contrasting with the furosemide- or thiazide-induced alkalosis (42). The physiologic role of cap1 is particularly intriguing. Cap1 acts to stimulate ENaC (14) while simultaneously inhibiting claudin-4 conductivity. Because aldosterone increases cap1 gene expression in the kidney (16), cap1 could fine-tune the CD from salt reabsorption to K^+ secretion. Notably, WNK4 plays an opposite role as cap1 by inhibiting ENaC (43), while at the same time augmenting paracellular Cl^- conductance (44). Because claudin-4 KO animals showed a slower reduction of urinary NaCl excretion but a steeper increase of aldosterone production when placed from a regular to a low-salt diet, aldosterone itself may regulate claudin-4 through cap1, WNK4, or other mechanisms. In a rat CD cell model, Le Moellic et al. first demonstrated that aldosterone stimulated claudin-4 protein phosphorylation and paracellular Cl^- permeability (45).

The mechanism of extracellular regulation of claudin is particularly important to the concept of a "druggable TJ." In general, low levels of trypsin and trypsin-like proteases such as cap1 and matriptase (cap3) are potent inducers of TJ formation in a variety of epithelia (25, 46–48). The constitutive cap1 KO mice died within 60 d after birth due to impaired skin barrier function and fatal dehydration (49). The TJ protein occludin was absent from the skin, leading to increased paracellular permeability to molecules <600 Da. Studies of cap3-null and hypomorphic mice have revealed leaky skin and gut barriers (48). The trypsin- and

cap3-induced barrier formation in the intestine was believed to implicate the E-cadherin and PKCζ signaling cascades through gene expression changes in claudin-2 and ZO-1 (47, 48). We have discovered that cap1 directly regulates claudin *trans* interaction. Loss of claudin interaction reduces its membrane stability, causing increased endocytosis. This mechanism is quick (within 1 h) and is exerted extracellularly, making it an attractive strategy for pharmacological intervention at the TJ level. Although the TJ architecture is not resolved, modern imaging approaches have revealed highly dynamic behaviors of the TJ comprising rapid opening/closing events that may reflect constant breaking and establishing of claudin interactions (50). Luminal proteases such as cap1 may contribute to such dynamic behavior of TJ or rely upon the opening event to gain access to its claudin targets. The *trans* claudin interaction depends upon its ECL2 domain, which consists of ∼25 amino acids with a helix–turn–helix motif (35) and also mediates claudin interactions with extracellular pathogens such as the *Clostridium perfringens* enterotoxin (51). Mutagenic screening in claudin-5 has identified three loci of amino acids in ECL2 (F147, Y148, and Y158) critical for its *trans* interaction (35). Notably, the Y158 site is homologous to the R158 site in claudin-4, critical for cap1-mediated dissociation. The R158 site is within a basic region flanked by a preceding lysine and, although not a perfect substrate, can be cleaved by cap1 in an in vitro fragment test (37). We had attempted to capture the cleaved species of claudin-4 in vivo in native M-1 and mIMCD3 or transfected HEK293 cells. In both the membrane fraction and whole-cell lysate, claudin-4 only existed as a single band of ∼21 kDa after cap1 treatments. Nevertheless, these data do not rule out the possibility that claudin-4 is cleaved in vivo by cap1 because of the transient nature of the intermediate species. We reckon that cap1 treatments in combination with blockers for endocytosis or ubiquitylation, although not within the scope of this study, may create a "frozen moment" for claudin-4 cleavage, allowing capture of the cleaved fragments and direct verification of its cleavage site with mass spectrometry.

Materials and Methods

The information on chemicals and reagents used in this study is summarized in *SI Appendix*, Table S4. All mice were bred and maintained according to the Washington University animal research requirements. All surgical procedures were approved by the Institutional Animal Research and Care committee. See *SI Appendix, Materials and Methods* for additional topics on generation of claudin-4 floxed animals, siRNA screening, molecular cloning and retrovirus production, recombinant cap1 protein production, immunolabeling and confocal microscopy, electrophysiological measurements, statistical analyses, and so forth.

ACKNOWLEDGMENTS. We thank Dr. Aubrey Morrison for helpful suggestions on this manuscript. We thank Jiaqi Zhang for maintaining and genotyping transgenic animals. We thank the Hope Center of Washington University for assistance on arterial BP measurements. We thank the cardiology center of Washington University for assistance on telemetric BP measurements. We thank the O'Brien Center of Washington University for assistance on electrolyte measurements. This work was supported by National Institutes of Health Grants RO1DK084059 (to J.H.) and P30 DK079333 (to J.H.) and by American Heart Association Grant 0930050N (to J.H.).

1. Kurtz TW, Morris RC, Jr (1983) Dietary chloride as a determinant of "sodium-dependent" hypertension. *Science* 222(4628):1139–1141.
2. Whitescarver SA, Ott CE, Jackson BA, Guthrie GP, Jr, Kotchen TA (1984) Salt-sensitive hypertension: Contribution of chloride. *Science* 223(4643):1430–1432.
3. Guyton AC (1991) Blood pressure control—Special role of the kidneys and body fluids. *Science* 252(5014):1813–1816.
4. Lifton RP, Gharavi AG, Geller DS (2001) Molecular mechanisms of human hypertension. *Cell* 104(4):545–556.
5. Reilly RF, Ellison DH (2000) Mammalian distal tubule: Physiology, pathophysiology, and molecular anatomy. *Physiol Rev* 80(1):277–313.
6. Royaux IE, et al. (2001) Pendrin, encoded by the Pendred syndrome gene, resides in the apical region of renal intercalated cells and mediates bicarbonate secretion. *Proc Natl Acad Sci USA* 98(7):4221–4226.
7. Leviel F, et al. (2010) The Na+-dependent chloride-bicarbonate exchanger SLC4A8 mediates an electroneutral Na+ reabsorption process in the renal cortical collecting ducts of mice. *J Clin Invest* 120(5):1627–1635.
8. Canessa CM, et al. (1994) Amiloride-sensitive epithelial Na+ channel is made of three homologous subunits. *Nature* 367(6462):463–467.
9. Kim YH, et al. (2007) Reduced ENaC protein abundance contributes to the lower blood pressure observed in pendrin-null mice. *Am J Physiol Renal Physiol* 293(4): F1314–F1324.
10. Pech V, et al. (2010) Pendrin modulates ENaC function by changing luminal HCO3-. *J Am Soc Nephrol* 21(11):1928–1941.
11. Hou J, Renigunta A, Yang J, Waldegger S (2010) Claudin-4 forms paracellular chloride channel in the kidney and requires claudin-8 for tight junction localization. *Proc Natl Acad Sci USA* 107(42):18010–18015.
12. Sansom SC, Weinman EJ, O'Neil RG (1984) Microelectrode assessment of chloride-conductive properties of cortical collecting duct. *Am J Physiol* 247(2 Pt 2):F291–F302.
13. Hou J, Rajagopal M, Yu AS (2013) Claudins and the kidney. *Annu Rev Physiol* 75: 479–501.
14. Vallet V, Chraibi A, Gaeggeler HP, Horisberger JD, Rossier BC (1997) An epithelial serine protease activates the amiloride-sensitive sodium channel. *Nature* 389(6651): 607–610.
15. Vuagniaux G, Vallet V, Jaeger NF, Hummler E, Rossier BC (2002) Synergistic activation of ENaC by three membrane-bound channel-activating serine proteases (mCAP1, mCAP2, and mCAP3) and serum- and glucocorticoid-regulated kinase (Sgk1) in Xenopus oocytes. *J Gen Physiol* 120(2):191–201.
16. Narikiyo T, et al. (2002) Regulation of prostasin by aldosterone in the kidney. *J Clin Invest* 109(3):401–408.
17. Furuse M, et al. (2002) Claudin-based tight junctions are crucial for the mammalian epidermal barrier: A lesson from claudin-1-deficient mice. *J Cell Biol* 156(6):1099–1111.
18. Katahira J, Inoue N, Horiguchi Y, Matsuda M, Sugimoto N (1997) Molecular cloning and functional characterization of the receptor for Clostridium perfringens enterotoxin. *J Cell Biol* 136(6):1239–1247.
19. Mitchell LA, Overgaard CE, Ward C, Margulies SS, Koval M (2011) Differential effects of claudin-3 and claudin-4 on alveolar epithelial barrier function. *Am J Physiol Lung Cell Mol Physiol* 301(1):L40–L49.
20. Fujita H, Hamazaki Y, Noda Y, Oshima M, Minato N (2012) Claudin-4 deficiency results in urothelial hyperplasia and lethal hydronephrosis. *PLoS ONE* 7(12):e52272.
21. Nielsen S, DiGiovanni SR, Christensen EI, Knepper MA, Harris HW (1993) Cellular and subcellular immunolocalization of vasopressin-regulated water channel in rat kidney. *Proc Natl Acad Sci USA* 90(24):11663–11667.
22. Christensen BM, et al. (2010) Sodium and potassium balance depends on αENaC expression in connecting tubule. *J Am Soc Nephrol* 21(11):1942–1951.
23. Ronzaud C, et al. (2007) Impairment of sodium balance in mice deficient in renal principal cell mineralocorticoid receptor. *J Am Soc Nephrol* 18(6):1679–1687.
24. Hansen PB, et al. (2004) Plasma renin in mice with one or two renin genes. *Acta Physiol Scand* 181(4):431–437.
25. Liu L, Hering-Smith KS, Schiro FR, Hamm LL (2002) Serine protease activity in m-1 cortical collecting duct cells. *Hypertension* 39(4):860–864.
26. Vuagniaux G, et al. (2000) Activation of the amiloride-sensitive epithelial sodium channel by the serine protease mCAP1 expressed in a mouse cortical collecting duct cell line. *J Am Soc Nephrol* 11(5):828–834.
27. Hou J, Paul DL, Goodenough DA (2005) Paracellin-1 and the modulation of ion selectivity of tight junctions. *J Cell Sci* 118(Pt 21):5109–5118.
28. Chen M, Chen LM, Lin CY, Chai KX (2010) Hepsin activates prostasin and cleaves the extracellular domain of the epidermal growth factor receptor. *Mol Cell Biochem* 337(1-2):259–266.
29. Verghese GM, Gutknecht MF, Caughey GH (2006) Prostasin regulates epithelial monolayer function: Cell-specific Gpld1-mediated secretion and functional role for GPI anchor. *Am J Physiol Cell Physiol* 291(6):C1258–C1270.
30. Déry O, Corvera CU, Steinhoff M, Bunnett NW (1998) Proteinase-activated receptors: Novel mechanisms of signaling by serine proteases. *Am J Physiol* 274(6 Pt 1): C1429–C1452.
31. Hou J, et al. (2008) Claudin-16 and claudin-19 interact and form a cation-selective tight junction complex. *J Clin Invest* 118(2):619–628.
32. Hou J, et al. (2009) Claudin-16 and claudin-19 interaction is required for their assembly into tight junctions and for renal reabsorption of magnesium. *Proc Natl Acad Sci USA* 106(36):15350–15355.
33. Furuse M, Sasaki H, Tsukita S (1999) Manner of interaction of heterogeneous claudin species within and between tight junction strands. *J Cell Biol* 147(4):891–903.
34. Daugherty BL, Ward C, Smith T, Ritzenthaler JD, Koval M (2007) Regulation of heterotypic claudin compatibility. *J Biol Chem* 282(41):30005–30013.
35. Piontek J, et al. (2008) Formation of tight junction: Determinants of homophilic interaction between classic claudins. *FASEB J* 22(1):146–158.
36. Kausalya PJ, et al. (2006) Disease-associated mutations affect intracellular traffic and paracellular Mg2+ transport function of Claudin-16. *J Clin Invest* 116(4):878–891.
37. Shipway A, et al. (2004) Biochemical characterization of prostasin, a channel activating protease. *Biochem Biophys Res Commun* 324(2):953–963.
38. Naguro I, et al. (2012) ASK3 responds to osmotic stress and regulates blood pressure by suppressing WNK1-SPAK/OSR1 signaling in the kidney. *Nat Commun* 3:1285.
39. Hadchouel J, et al. (2010) Decreased ENaC expression compensates the increased NCC activity following inactivation of the kidney-specific isoform of WNK1 and prevents hypertension. *Proc Natl Acad Sci USA* 107(42):18109–18114.

40. Doi M, et al. (2010) Salt-sensitive hypertension in circadian clock-deficient Cry-null mice involves dysregulated adrenal Hsd3b6. *Nat Med* 16(1):67–74.
41. Garella S, Cohen JJ, Northrup TE (1991) Chloride-depletion metabolic alkalosis induces ECF volume depletion via internal fluid shifts in nephrectomized dogs. *Eur J Clin Invest* 21(3):273–279.
42. Galla JH (2000) Metabolic alkalosis. *J Am Soc Nephrol* 11(2):369–375.
43. Ring AM, et al. (2007) WNK4 regulates activity of the epithelial Na+ channel in vitro and in vivo. *Proc Natl Acad Sci USA* 104(10):4020–4024.
44. Kahle KT, et al. (2004) Paracellular Cl- permeability is regulated by WNK4 kinase: Insight into normal physiology and hypertension. *Proc Natl Acad Sci USA* 101(41): 14877–14882.
45. Le Moellic C, et al. (2005) Aldosterone and tight junctions: Modulation of claudin-4 phosphorylation in renal collecting duct cells. *Am J Physiol Cell Physiol* 289(6): C1513–C1521.
46. Swystun VA, et al. (2009) Serine proteases decrease intestinal epithelial ion permeability by activation of protein kinase Czeta. *Am J Physiol Gastrointest Liver Physiol* 297(1):G60–G70.
47. Buzza MS, et al. (2013) Prostasin is required for matriptase activation in intestinal epithelial cells to regulate closure of the paracellular pathway. *J Biol Chem* 288(15):10328–10337.
48. Buzza MS, et al. (2010) Membrane-anchored serine protease matriptase regulates epithelial barrier formation and permeability in the intestine. *Proc Natl Acad Sci USA* 107(9):4200–4205.
49. Leyvraz C, et al. (2005) The epidermal barrier function is dependent on the serine protease CAP1/Prss8. *J Cell Biol* 170(3):487–496.
50. Shen L, Weber CR, Raleigh DR, Yu D, Turner JR (2011) Tight junction pore and leak pathways: A dynamic duo. *Annu Rev Physiol* 73:283–309.
51. Veshnyakova A, et al. (2012) Mechanism of Clostridium perfringens enterotoxin interaction with claudin-3/-4 protein suggests structural modifications of the toxin to target specific claudins. *J Biol Chem* 287(3):1698–1708.